

Central exclusive diffractive production as a spin–parity analyser: from hadrons to Higgs

A.B. KAIDALOV^{a,b}, V.A. KHOZE^{a,c}, A.D. MARTIN^a AND M.G. RYSKIN^{a,c}

^a Department of Physics and Institute for Particle Physics Phenomenology,
University of Durham, DH1 3LE, UK

^b Institute of Theoretical and Experimental Physics, Moscow, 117259, Russia

^c Petersburg Nuclear Physics Institute, Gatchina, St. Petersburg, 188300, Russia

Abstract

We present the general rules for double-Reggeon production of objects with different spins and parities. The existing experimental information on resonance production in these central exclusive diffractive processes is discussed. The absorptive corrections are calculated and found to depend strongly on the quantum numbers of the produced states. The central exclusive diffractive production of 0^+ and 0^- Higgs bosons is studied as an illustrative topical example of the use of the general rules. The signal for diffractive 0^+ and 0^- Higgs production at the LHC is evaluated using, as an example, the minimal supersymmetric model, with large $\tan\beta$.

1 Introduction

It is always a challenge to measure the quantum numbers of new states, particularly their spin and parity. We may measure the specific characteristics of given decay channels or angular correlations of the accompanying particles in the production process, especially the correlations between the outgoing protons in the central exclusive production process, $pp \rightarrow p+h+p$, shown in Fig. 1(a). The advantage of the latter approach is that it offers the possibility, not only to separate different states by accurately measuring the missing mass, but also to distinguish between scalar and pseudoscalar new heavy objects, which is difficult from studying their decay products. In this paper we begin by studying the general implications of applying Reggeon

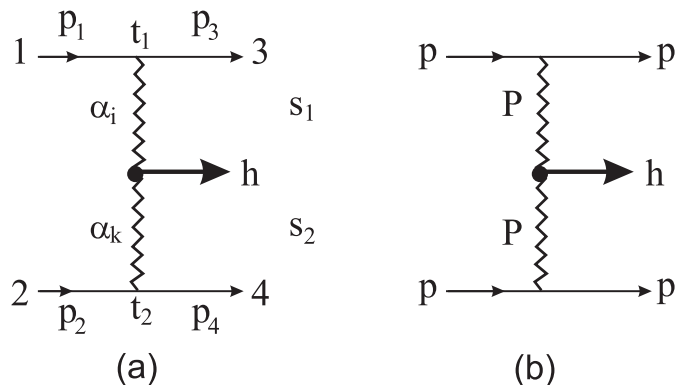


Figure 1: (a) The central production of a state h by double-Reggeon exchange. (b) The double-Pomeron exchange contribution to $pp \rightarrow p + h + p$, which dominates at high energies, where the $+$ signs are used to indicate the presence of Pomeron-induced rapidity gaps.

techniques to describe such exclusive processes. At very high energies, and in the central region ($x_F \simeq 0$), the double-Pomeron process, Fig 1(b), should give the dominant contribution.

The theory of double-Reggeon (and multi-Reggeon) exchanges was developed long ago [1]. However the revival of interest in these processes is related to the new effects observed in the central production of resonances by the WA102 experiment [2] in the reaction $pp \rightarrow pX^0p$, and to the proposal to look for the Higgs boson and other new particles in double-Pomeron-exchange processes, see, for example, [3]–[7]. Indeed it will be one of the main challenges of the LHC to identify the nature (including the spin–parity) of newly-discovered heavy objects. It appears to be very hard to find a spin–parity analyser using conventional approaches.

Models for double-Pomeron-exchange production of hadrons with different quantum numbers have been developed in recent years [8]–[13]. However in some papers [9, 10] the formulas of Reggeon theory were not fully consistent, while some results of the others follow simply from general rules of the Reggeon approach. In Section 2 we first consider these rules and compare them with experimental observations [2], and with the results of the phenomenological analysis performed in Ref. [12]. Also the dynamics for the Pomeron–Pomeron–particle vertices is discussed.

In Section 3 we illustrate how the general behaviour is distorted by the dynamics of the process, using $h(0^\pm)$ exclusive diffractive production as an example. Apart from subsection 3.1, where we discuss the uncertainties in the predicted cross sections, this section neglects the absorptive or unitary corrections. However at high energies these corrections are important (see, for example, Refs. [14]–[18]). They correspond to the diagrams of Fig. 2, and can be calculated using the Reggeon diagram technique [19]. It will be shown in Section 4 that the inclusion of these diagrams leads not only to a decrease of the cross sections of the double-Pomeron processes, but also to significant modifications of the angular correlations between the

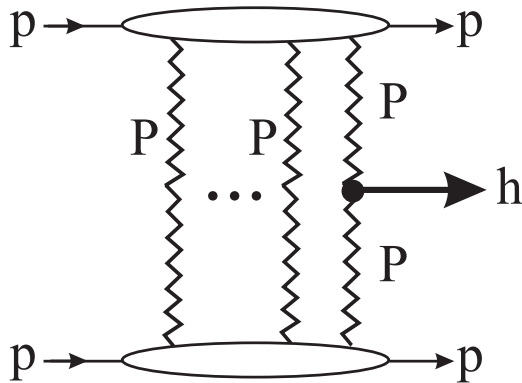


Figure 2: Unitarity or rescattering corrections to the exclusive diffractive process $pp \rightarrow p+h+p$.

outgoing (forward) protons. Moreover, the magnitude of these absorptive corrections depends on the quantum numbers of the produced state h .

In Section 4 we illustrate the results using the important topical example of the double-Pomeron production of heavy bosons. In particular we compare the production of a Standard Model Higgs boson with spin-parity $J^P = 0^+$, with that for a 0^- Higgs¹ which appears in various extensions of the Standard Model, in particular in a supersymmetric extension. In Section 5, we consider the consequences of this approach to investigations of the Higgs sector at the LHC. For illustration we evaluate the exclusive cross sections using the minimal supersymmetric model² (MSSM) with large $\tan \beta$; a domain in which, for $m(0^-) \lesssim 200$ GeV, the conventional searches at the LHC will face difficulties to discriminate between the different Higgs states and to determine their masses. This is especially true in the so-called “intense coupling limit”, $m_h \sim m_A \sim m_H \sim \mathcal{O}(100 \text{ GeV})$ [21]. As a specific example we calculate the event rates for the exclusive central production of mass 115 GeV 0^\pm bosons at the LHC.

2 Exclusive diffractive production: general rules

Here we study the general rules for the amplitudes of the exclusive diffractive process

$$1 + 2 \rightarrow 3 + h + 4, \quad (1)$$

shown in Fig. 1, where $1, \dots, 4$ are hadrons, and where the centrally produced particle h has spin and parity J^P . We show that the production process has characteristic features, that depend on the value of J^P , which follow from general principles.

¹For convenience of presentation we will denote this particle $h(0^-)$, rather than the conventional notation $A(0^-)$.

²For a recent review see, for example, Ref. [20].

To begin, we assume that all the particles are spinless. Then, at high energies and small momentum transfer,

$$\begin{aligned} s_1 &= (p_3 + p_h)^2 \gg s_0, & s_2 &= (p_4 + p_h)^2 \gg s_0 \\ t_1 &\simeq -p_{3\perp}^2 \lesssim s_0, & t_2 &\simeq -p_{4\perp}^2 \lesssim s_0, \end{aligned} \quad (2)$$

the amplitude can be written in the form [1]

$$T_{12}^{3h4}(s_1, s_2, \vec{p}_{3\perp}, \vec{p}_{4\perp}) = \sum_{i,k} g_{13}(t_1) g_{24}(t_2) \left(\frac{s_1}{s_0}\right)^{\alpha_i(t_1)} \left(\frac{s_2}{s_0}\right)^{\alpha_k(t_2)} \eta(\alpha_i(t_1)) \eta(\alpha_k(t_2)) g_{ik}^h(t_1, t_2, \phi), \quad (3)$$

where $s_0 = 1 \text{ GeV}^2$, ϕ is the angle between the transverse momenta $\vec{p}_{3\perp}$ and $\vec{p}_{4\perp}$ of the outgoing protons and

$$\eta(\alpha_i(t)) = - \left(\frac{1 + \sigma_i e^{-i\pi\alpha_i(t)}}{\sin \pi\alpha_i(t)} \right) \quad (4)$$

is the signature factor for Regge pole i with trajectory $\alpha_i(t)$ and signature $\sigma_i = \pm 1$. The vertex factors $g_{13}(t_1)$ and $g_{24}(t_2)$ describe the $13 - \alpha_i$ and $24 - \alpha_k$ couplings respectively, while g_{ik}^h describes the transition $\alpha_i\alpha_k \rightarrow h$. Note that g_{ik}^h depends, in general, on all the scalars that can be formed from the vectors which enter the vertex. Moreover, in the case of Reggeons, the longitudinal and transverse components of their momenta act as two different vectors [19]. In our case, where the mass of the boson h is fixed, it is enough to keep the transverse momenta $\vec{p}_{3\perp}$ and $\vec{p}_{4\perp}$, and the unit vector \vec{n}_0 in the direction of the colliding hadrons. Unlike g_{13} and g_{24} , the function g_{ik}^h may be complex. In the Regge domain (2),

$$s_1 s_2 = s(m_h^2 + p_{h\perp}^2), \quad (5)$$

where $s = (p_1 + p_2)^2$.

When spin is included, the process is described by helicity amplitudes, each of which has a double-Regge behaviour as in (3) [22].

$$T_{\lambda_1\lambda_2}^{\lambda_3\lambda_h\lambda_4}(s_1, s_2, t_1, t_2, \phi) = \sum_{i,k} g_{\lambda_1\lambda_3}(t_1) g_{\lambda_2\lambda_4}(t_2) \left(\frac{s_1}{s_0}\right)^{\alpha_i(t_1)} \left(\frac{s_2}{s_0}\right)^{\alpha_k(t_2)} \eta(\alpha_i(t_1)) \eta(\alpha_k(t_2)) g_{ik}^{\lambda_h}(t_1, t_2, \phi) \quad (6)$$

The relations between the vertex couplings for different helicities, due to conservation of parity and other quantum numbers, are the same as for $2 \rightarrow 2$ reaction [23]. For example,

$$g_{\lambda_1\lambda_3}(t) = (-1)^{\lambda_1 - \lambda_3} \xi_1 g_{-\lambda_1 - \lambda_3}(t), \quad (7)$$

with

$$\xi_1 = \eta_1 \eta_3 (-1)^{S_1 - S_3} P_i \sigma_i, \quad (8)$$

where S_1 (S_3) and η_1 (η_3) are the spin and parity of the particle 1 (3) respectively, and P_i, σ_i are the parity and signature of the Reggeon i . The vertices behave as [23, 24],

$$g_{\lambda_1\lambda_3}(t) \sim (-t)^{|\lambda_1 - \lambda_3|/2}, \quad \text{as } t \rightarrow 0. \quad (9)$$

Note that relation (7) depends only on the product $P_i\sigma_i$ and thus the model-independent spin structure of the vertices $g_{\lambda_1\lambda_3}(g_{\lambda_2\lambda_4})$ is the same for all Reggeons with the same product $P_i\sigma_i$.

Below we will be interested mainly in the spin structure of the central vertex $g_{ik}^{\lambda_h}(t_1, t_2, \phi)$. It can be written in the form [22]

$$g_{ik}^{\lambda_h} = \sum_{m_2=-\infty}^{\infty} e^{im_2\phi} \gamma_{m_1 m_2}^{\lambda_h}, \quad \text{with } m_1 + m_2 = \lambda_h, \quad (10)$$

where m_2 has the meaning of the projection of the angular momentum j_k of Reggeon k (analytically continued from all angular momenta j_k in the t_1, t_2 -channels). Now invariance under parity leads to the relation [22]

$$\gamma_{m_1 m_2}^{\lambda_h} = (-1)^{\lambda_h} \xi_3 \gamma_{-m_1 - m_2}^{-\lambda_h}, \quad (11)$$

where

$$\xi_3 = \eta_h (-1)^{S_h} P_i \sigma_i P_k \sigma_k. \quad (12)$$

Thus the spin structure of the central vertex depends only on the product of the naturalities (that is the parities and signatures) of particle h and the exchanged Reggeons³. The behaviour of $\gamma_{m_1 m_2}^{\lambda_h}$ for small t_1, t_2 is given by the formula [22]

$$\gamma_{m_1 m_2}^{\lambda_h} \sim (-t_1)^{|m_1|/2} (-t_2)^{|m_2|/2}, \quad \text{with } m_1 + m_2 = \lambda_h. \quad (13)$$

Note that all values of m_2 (m_1) enter (10), but, due to (13), for small t_1, t_2 it is enough to consider the lowest values of m_2 (m_1) consistent with (11).

It is often convenient to write the spin structure of the amplitudes in terms of the characteristic 3-vectors of the problem. Such a representation is closely related to the helicity amplitudes discussed above [24], but the formulas become more transparent. In this case the central vertex g_{ik}^h is written as a scalar (or pseudoscalar) function (depending on the product $\eta_h (-1)^{S_h} \sigma_i P_i \sigma_k P_k$) of the vectors $\vec{p}_{3\perp}, \vec{p}_{4\perp}$ and the spin vectors (tensors) of particle h .

Let us consider particular examples for the spin-parity J^P of h , in each case taking $\sigma_i P_i \sigma_k P_k = +1$ as for double-Pomeron exchange.

(a) $J^P(h) = 0^+$

For a scalar particle h , the vertex coupling is simply

$$g_{ik}^h = f_{0^+}(p_{3\perp}^2, p_{4\perp}^2, \vec{p}_{3\perp} \cdot \vec{p}_{4\perp}), \quad (14)$$

where f_{0^+} is a function of the scalar variables which can be formed from the transverse momenta $\vec{p}_{3\perp}$ and $\vec{p}_{4\perp}$ of the outgoing protons. When $\vec{p}_{3\perp}$ or $\vec{p}_{4\perp} \rightarrow 0$, this function in general tends to some constant $f(0, 0, 0)$. In order to obtain further information on the structure of this function, extra dynamical input is needed (see Section 3).

³It can be shown that similar formulae are also valid for photon-photon fusion processes.

(b) $J^P(h) = 0^-$

For the central production of a pseudoscalar particle, the vertex factor takes the form

$$g_{ik}^h = f_{0^-}(p_{3\perp}^2, p_{4\perp}^2, \vec{p}_{3\perp} \cdot \vec{p}_{4\perp}) \varepsilon_{ikl}(p_{3\perp})_i (p_{4\perp})_k (n_0)_l, \quad (15)$$

where \vec{n}_0 is the unit vector in the direction of the colliding hadrons (in the c.m.s.). In this case, according to (11), all amplitudes with $m_1, m_2 = 0$ are zero, and so $|m_1| = |m_2| = 1$ are the leading terms. According to (13) this corresponds to helicity amplitudes which are proportional to $(-t_1)^{\frac{1}{2}}(-t_2)^{\frac{1}{2}}$ for small t . Thus the cross section behaves as $\sim |t_1||t_2|$. Also the angular distribution contains a factor $\sin^2 \phi$, which is evident from either (15) or (10) and (11). Again the function f_{0^-} is not predicted from general principles.

Note that the characteristic $\sin^2 \phi$ dependence of the angular distribution, and the t -behaviour at small t , which are observed by the WA102 Collaboration for η , and η' production [2], are direct consequences of the general properties of the double-Regge-exchange amplitudes. This behaviour is valid not only for double-Pomeron exchange, but also for $Pf, ff, \rho\rho, A_2A_2, \omega\omega, \dots$ exchanges. Under the interchange of the Reggeons, $i \leftrightarrow k$,

$$(n_0)_l \rightarrow -(n_0)_l \quad (16)$$

and hence if the Reggeons are the same, $i = k$, the function f_{0^-} should be symmetric under the interchange $3 \leftrightarrow 4$.

(c) $J^P(h) = 1^+$

For the production of an axial vector state, both $\lambda_h = 0$ and $\lambda_h = \pm 1$ components are present, and the vertex factor can be written as

$$g_{ik}^h = f_{1^+}^0 \varepsilon_{ikl}(p_{3\perp})_i (p_{4\perp})_k e_l + \left(f_{1^+}^1 (p_{3\perp})_i + \tilde{f}_{1^+}^1 (p_{4\perp})_i \right) \varepsilon_{ikl}(n_0)_k e_l, \quad (17)$$

where the f^i are functions of the scalar variables $p_{3\perp}^2, p_{4\perp}^2$ and $\vec{p}_{3\perp} \cdot \vec{p}_{4\perp}$, and where \vec{e} is the polarization vector of the 1^+ meson. If both of the exchanged Reggeons are the same ($i = k$), then the function g_{ik}^h is symmetric under the interchange $3 \leftrightarrow 4$. As a consequence, for small $\vec{p}_{i\perp}$,

$$f_{1^+}^0 \sim (p_{3\perp}^2 - p_{4\perp}^2), \quad f_{1^+}^1 = -\tilde{f}_{1^+}^1. \quad (18)$$

The form of the vertex factors g_{ik}^h for the central production of states h of higher spin can readily be constructed using equations (10)–(12).

It is interesting to note that the structure of the vertex factors given in (14)–(18) coincides, for small $\vec{p}_{i\perp}$, with that found using a non-conserved vector current model [12], which gives a good description of the experimental data of the WA102 Collaboration [2]. However, from the discussion above, it is clear that these results simply follow from the general rules of Reggeon theory. They are not connected with a particular vector current model of the Pomeron, but

rather follow from the fact that the product of the parity and signature of the Pomeron is $+1$. Moreover the Pomeron has positive signature and corresponds to the analytic continuation from angular momenta $J^P = 2^+, 4^+, \dots$ in the t -channel. The same results would be obtained if a tensor current model were used.

On the other hand, the detailed structure of the amplitudes $f_m^k(p_{3\perp}^2, p_{4\perp}^2, \vec{p}_{3\perp} \cdot \vec{p}_{4\perp})$ (with $m = 0^+, 0^-, 1^+, 2^+, \dots$) depends on dynamics and cannot be predicted from the general principles of Regge theory. For example, if the heavy state h is strongly coupled to gluons and is produced perturbatively via the diagram shown in Fig. 3(a), then in the forward direction ($p_{3\perp}, p_{4\perp} \ll Q_\perp$) the vertex factor f_{0^+} does not depend on p_3 or p_4 . Moreover, as was shown in [25, 26, 7], there exists a $J_z = 0$, parity-even, selection rule, for production by gluon–gluon fusion where each of these active gluons comes from colour-singlet digluon t -channel exchange, see Fig. 3. As a consequence the production of the negative-parity $h(0^-)$ state is strongly suppressed in comparison with the production of the $h(0^+)$ state. Similarly it follows that the central diffractive exclusive production of 2^{++} states is also suppressed in some topical cases; for example, 2^{++} states formed from heavy quark pairs (in the non-relativistic model) [26, 27] or 2^{++} ‘gravitons’ in models with extra dimensions in which their coupling to gluons has a point-like nature (with no derivatives) so they are not produced via the $J_z = 0$ two-gluon state [7]. Also these processes can provide a unique opportunity to determine the quantum numbers of pair-produced new strongly-interacting objects [7]. For example, comparatively light gluinos and squarks can be distinguished by the respective β^3 and β threshold behaviour, where β is the particle velocity.

3 Example: dynamics of $h(0^\pm)$ Higgs production

So far we have discussed the structure of the production amplitudes for

$$pp \rightarrow p + h + p, \tag{19}$$

where h has a given J^P , which follow from general principles. To go further we need to consider the dynamics of the process. We study $h(0^\pm)$ Higgs production as a topical example. The general rules imply that the central vertices behave as

$$\begin{aligned} g_{ik}^{h(0^+)} &\sim \text{constant} \\ g_{ik}^{h(0^-)} &\sim (\vec{p}_{3\perp} \times \vec{p}_{4\perp}) \cdot \vec{n}_0 \sim |t_1|^{\frac{1}{2}} |t_2|^{\frac{1}{2}} \sin \phi \end{aligned} \tag{20}$$

at small t .

3.1 Amplitudes for $h(0^\pm)$ production

To see how the dynamics modify this behaviour we have first to describe how the cross sections for the exclusive production of $h(0^\pm)$ Higgs bosons are calculated. We use the formalism of

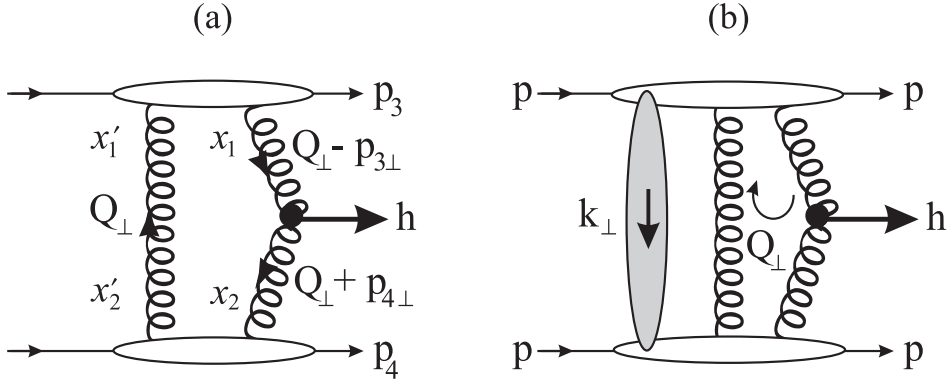


Figure 3: (a) The QCD diagram for double-diffractive exclusive production of a Higgs boson h , $pp \rightarrow p + h + p$, where the gluons of the hard subprocess $gg \rightarrow h$ are colour screened by the second t -channel gluon. (b) The rescattering or absorptive corrections to $pp \rightarrow p + h + p$, where the shaded region represents the multi-Pomeron exchanges of Fig. 2.

Ref. [6, 26, 7]. The amplitudes are described by the diagram shown in Fig. 3(a), where the hard subprocesses $gg \rightarrow h(0^\pm)$ are initiated by gluon–gluon fusion and where the second t -channel gluon is needed to screen the colour flow across the rapidity gap intervals. The Born amplitudes are of the form

$$T_h = N \int \frac{d^2 Q_\perp V_h}{Q_\perp^2 (\vec{Q}_\perp - \vec{p}_{3\perp})^2 (\vec{Q}_\perp + \vec{p}_{4\perp})^2} f_g(x_1, x'_1, Q_3^2, \mu^2; t_1) f_g(x_2, x'_2, Q_4^2, \mu^2; t_2) \quad (21)$$

The overall normalization constant N can be written in terms of the $h \rightarrow gg$ decay width [7], and the $gg \rightarrow h$ vertex factors are

$$\begin{aligned} V_{h(0^+)} &= (\vec{Q}_\perp - \vec{p}_{3\perp}) \cdot (\vec{Q}_\perp + \vec{p}_{4\perp}) \\ V_{h(0^-)} &= ((\vec{Q}_\perp - \vec{p}_{3\perp}) \times (\vec{Q}_\perp + \vec{p}_{4\perp})) \cdot \vec{n}_0. \end{aligned} \quad (22)$$

The f_g 's are the skewed unintegrated gluon densities of the proton at the hard scale μ , taken to be $m_h/2$, with

$$\begin{aligned} Q_3 &= \min \left\{ Q_\perp, |(\vec{Q}_\perp - \vec{p}_{3\perp})| \right\}, \\ Q_4 &= \min \left\{ Q_\perp, |(\vec{Q}_\perp + \vec{p}_{4\perp})| \right\}. \end{aligned} \quad (23)$$

Below, we assume factorization of the unintegrated distributions,

$$f_g(x, x', Q^2, \mu^2; t) = f_g(x, x', Q^2, \mu^2) F_N(t), \quad (24)$$

where we parameterize the form factor of the proton vertex by the form $F_N(t) = \exp(bt)$ with $b = 2 \text{ GeV}^{-2}$. To single log accuracy, we have [28]

$$f_g(x, x', Q_i^2, \mu^2) = R_g \frac{\partial}{\partial \ln Q_i^2} \left(\sqrt{T(Q_i, \mu)} xg(x, Q_i^2) \right), \quad (25)$$

where T is the usual Sudakov form factor which ensures that the gluon remains untouched in the evolution up to the hard scale μ , so that the rapidity gaps survive. The square root arises because the bremsstrahlung survival probability T is only relevant to the hard gluon. R_g is the ratio of the skewed $x' \ll x$ integrated distribution to the conventional diagonal density $g(x, Q^2)$. For $x \ll 1$ it is completely determined [29]. The apparent infrared divergence of (21) is nullified⁴ for $h(0^+)$ production by the Sudakov factors embodied in the gluon densities f_g . However the amplitude for $h(0^-)$ production is much more sensitive to the infrared contribution. Indeed let us consider the case of small $p_{i\perp}$ of the outgoing protons. Then, from (22), we see that $V_{h(0^+)} \sim Q_\perp^2$, whereas $V_{h(0^-)} \sim p_{3\perp}p_{4\perp}$ (since the linear contribution in Q_\perp vanishes after the angular integration). Thus the d^2Q_\perp/Q_\perp^4 integration for $h(0^+)$ is replaced by $p_{3\perp}p_{4\perp}d^2Q_\perp/Q_\perp^6$ for $h(0^-)$, and now the Sudakov suppression is not enough to prevent a significant contribution from the $Q_\perp^2 \lesssim 1 \text{ GeV}^2$ domain.

3.2 Uncertainties

To estimate the uncertainty in the predictions for the $h^\pm(0)$ exclusive diffractive cross sections we first quantify the above uncertainty arising from the infrared region, where the gluon distribution is not well known. Fig. 4 shows the ϕ dependence of $h(0^-)$ and $h(0^+)$ production at the LHC, for $m_h = 120 \text{ GeV}$ and $\mu = m_h/2$, using different treatments of the infrared region. The continuous and dashed curves are calculated using MRST99 [30] and CTEQ6M [31] partons respectively with the very low Q gluon frozen at its value at $Q_{3,4} = 1.3 \text{ GeV}$. Then we integrate down in Q_\perp until $Q_{3,4}$ are close to Λ_{QCD} , where the contribution vanishes due to the presence of the T -factor. This will slightly overestimate the cross sections as the gluon density decreases with decreasing Q^2 for $x \sim 0.01$. A lower extreme is to remove the contribution below $Q_{3,4} = 1.3 \text{ GeV}$ entirely. The result for MRST99 partons is shown by the dotted curve in Fig. 4. Even with this extreme choice, the 0^+ cross section is not changed greatly; it is depleted by about 20%. On the other hand, as anticipated, we see for 0^- production, the infrared region is much more important and the cut reduces the cross section by a factor of 5.

Another uncertainty is the choice of factorization scale μ . Note that in comparison with previous calculations [7], which were done in the limit of proton transverse momenta, $p_{3,4\perp} \ll Q_\perp$, now we include the explicit p_\perp -dependence in the Q_\perp -loop integral of (21). Moreover, we resum the ‘soft’ gluon logarithms, $\ln 1/(1-z)$, in the T -factor.⁵ So now the T -factor includes both the single soft logarithms and the single collinear logarithms. The only uncertainty is the non-logarithmic NLO contribution. This may be modelled by changing the factorization scale,

⁴In addition, at LHC energies, the effective anomalous dimension of the gluon gives an extra suppression of the contribution from the low Q_\perp domain [4].

⁵To account for the interference and the precise form of the amplitude for soft gluon ($q_\perp \ll m_h$) large-angle emission, we explicitly calculate the one-loop virtual correction to the $gg \rightarrow h$ vertex, integrating over the whole angular range for $q_\perp \ll m_h$. We adjust the upper limit of the z -integral so that $z < 0.62m_h/(0.62m_h + q_\perp)$ in the expression for the T -factor (see eq. (10) of [7] with $k_t = q_\perp$), in order to reproduce the complete one-loop result.

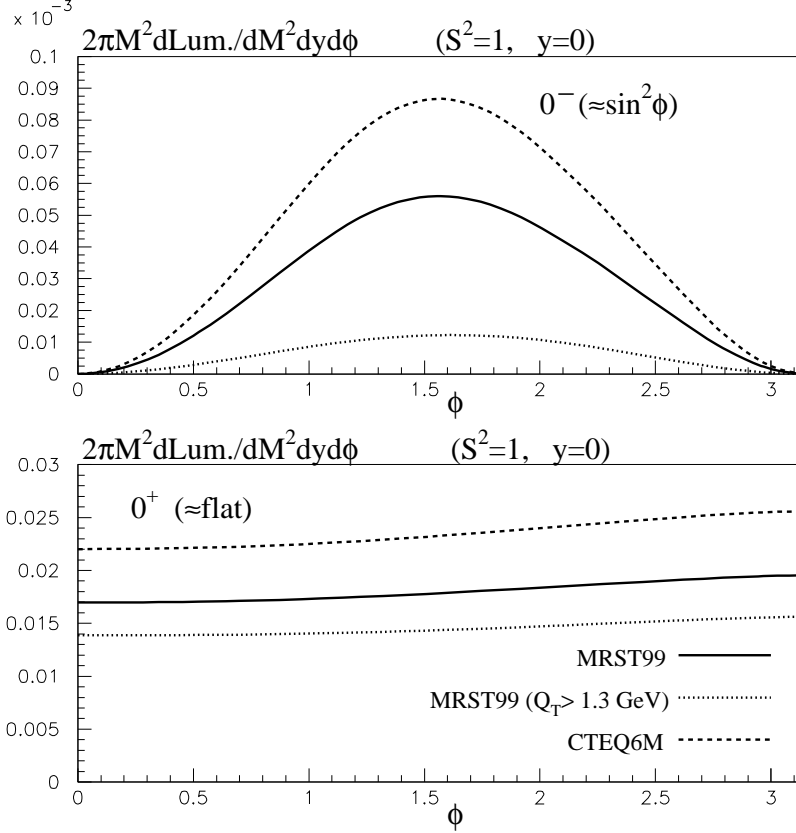


Figure 4: The ϕ dependences of diffractive exclusive $h(0^+)$ and $A(0^-) \equiv h(0^-)$ production, $pp \rightarrow p + h + p$, at the LHC, with $m_h = 120$ GeV. ϕ is the angle in the transverse plane between the outgoing protons. The curves are for central rapidity and do not include absorptive corrections. They correspond to the effective luminosities for the $gg \rightarrow h(0^\pm)$ subprocesses integrated over the outgoing proton momenta $\vec{p}_{i\perp}$, assuming an $\exp(-bp_{i\perp}^2)$ behaviour of the unintegrated gluon densities f_g , with slope $b = 2$ GeV $^{-2}$.

μ , which fixes the maximal q_\perp of the gluon in the NLO loop correction. As the default we have used $\mu = m_h/2$; that is the largest q_\perp allowed in the process with total energy m_h . Choosing a lower scale $\mu = m_h/4$ would enlarge the cross sections by about 30%.

Next there is some uncertainty in the gluon distribution itself. To illustrate this, we compare predictions obtained using CTEQ6M [31], MRST99 [30] and MRST02 [32] partons. For 0^+ production at the LHC, with $m_h = 120$ GeV and $\mu = m_h/2$, we find that the effective gluon-gluon luminosity, before screening, is

$$\left. \frac{d\mathcal{L}}{dy d \ln M^2} \right|_{y=0} = (2.2, 1.7, 1.45) \times 10^{-2} \quad (26)$$

respectively. This spread of values arises because the CTEQ gluon is 7% higher, and the MRST02 gluon 4% lower, than the default MRST99 gluon, in the relevant kinematic region. The sensitivity to the gluon arises because the central exclusive diffractive cross section is proportional to the 4th power of the gluon. For 0^- production, the corresponding numbers are $(4.2, 2.7, 1.7) \times 10^{-5}$. Up to now, we have discussed the effective gluon–gluon luminosity. However, NNLO corrections may occur in the $gg \rightarrow h$ fusion vertex. These give an extra uncertainty of $\pm 20\%$. Note that we have already accounted for the NLO corrections for this vertex [7].

Finally, we need to consider the uncertainty in the evaluation of the soft rescattering correction factor S^2 , which is the probability that the rapidity gaps survive the soft pp interaction. The computation of S^2 is discussed in some detail in Section 4. Here it suffices to say, from the analysis [16] of all soft pp data, that a conservative error on the values of S^2 is $\pm 50\%$.

Combining together all these sources of error we find that the prediction for the 0^+ cross section is uncertain to a factor of almost 2.5, that is up to almost 2.5, and down almost to $1/2.5$, times the default value.⁶ On the other hand, 0^- production is uncertain by this factor just from the first (infrared) source of error, with the remaining errors contributing almost another factor of 2.5. Although the rate of $h(0^-)$ production is very sensitive to the infrared contribution, and could indicate the presence of a significant non-perturbative contribution, we find that the form of the ϕ dependence is not. We discuss this point in Section 5.

Note that the non-local structure of the amplitude leads to an extra angular dependence coming from the correlations between \vec{Q}_\perp and the $\vec{p}_{i\perp}$ in the integral in (21). In fact, expanding the gluon propagators gives corrections of the type

$$\vec{Q}_\perp \cdot \vec{p}_{3\perp}/Q_\perp^2, \quad \vec{Q}_\perp \cdot \vec{p}_{4\perp}/Q_\perp^2, \quad (27)$$

which lead to an additional contribution of the form $-\vec{p}_{3\perp} \cdot \vec{p}_{4\perp}/Q_\perp^2$. This reflects the dependence of the vertex factors f_{0^\pm} on $\vec{p}_{3\perp} \cdot \vec{p}_{4\perp}$, see (14) and (15). However, it is evident from Fig. 4 that this contribution does not give a large effect. What is more important is the suppression of $h(0^-)$ production in comparison to that for $h(0^+)$. The $h(0^-)$ amplitude is proportional to $\vec{p}_{3\perp} \times \vec{p}_{4\perp}$, where the dimensions must be compensated by some scale. In perturbative QCD this is the scale Q_\perp^2 arising from the gluon loop in Fig. 3(a). Therefore the $h(0^-)$ cross section is reduced by a factor $\langle p_{3\perp}^2 p_{4\perp}^2 / 2Q_\perp^4 \rangle$, that is by a factor of the order of 500 for typical $p_{i\perp}^2 \sim 1/2b \sim 0.25 \text{ GeV}^2$ if $Q_\perp^2 \sim 4 \text{ GeV}^2$.

4 Absorptive corrections

In this section we consider how exclusive double-diffractive production is influenced by the absorptive (shadowing) effects, which arise from the multi-Pomeron diagrams of Fig. 2. To determine the suppression due to these absorptive corrections, it is convenient to work in impact parameter, b , space.

⁶For example, we predict the cross section for the exclusive diffractive production of a Standard Model Higgs at the LHC, with $m_h = 120 \text{ GeV}$, to be in the range 0.9–5.5 fb.

4.1 Absorptive effects for $h(0^+)$ production

The amplitude for the central production of an $h(0^+)$ state, via the double-Pomeron-exchange process $pp \rightarrow p + h + p$, has the form

$$T^h(s, \vec{b}_1, \vec{b}_2, \vec{b}) = \exp\left(-\frac{1}{2}\Omega_P(s, b^2)\right) T_{PP}^h(s_1, s_2, \vec{b}_1, \vec{b}_2), \quad (28)$$

where Ω_P is the contribution of Pomeron exchange to elastic pp scattering in impact parameter space

$$\Omega_P(s, b^2) = \frac{\sigma_{pp}^P}{4\pi B} \exp(-b^2/4B), \quad (29)$$

where σ_{pp}^P is the Pomeron contribution to the total cross section of the pp interaction, and

$$B = \frac{1}{2}B_0 + \alpha'_P \ln(s/s_0) \quad (30)$$

is the slope of the elastic pp amplitude. The amplitude T_{PP}^h is the Fourier transform, to impact-parameter space, of the amplitude $T_{12}^{3h4}(s_1, s_2, \vec{p}_{3\perp}, \vec{p}_{4\perp})$ of (1) with $i = k = P$. That is

$$T_{PP}^h(s_1, s_2, \vec{b}_1, \vec{b}_2) = \left(\frac{1}{2\pi}\right)^2 \int d^2p_{3\perp} d^2p_{4\perp} e^{i\vec{p}_{3\perp} \cdot \vec{b}_1} e^{-i\vec{p}_{4\perp} \cdot \vec{b}_2} T_{PP}^h(s_1, s_2, \vec{p}_{3\perp}, \vec{p}_{4\perp}), \quad (31)$$

where $\vec{b} = \vec{b}_1 + \vec{b}_2$ is the Fourier conjugate to $\vec{q} = \vec{p}_{3\perp} - \vec{p}_{4\perp}$. For simplicity, we give the formula for a single-channel eikonal, where only intermediate proton states are considered, between the Pomeron exchanges in Fig. 2. The extension to the multichannel case is straightforward. In the calculations presented here we used the two-channel eikonal model of Ref. [16].

Note that if $\alpha_P(0) - 1 \equiv \Delta > 0$, then $\Omega_P(s, b^2)$ increases with energy and leads to a substantial suppression of cross section at very high energies. Calculations, using the model of Ref. [16], show that at Tevatron energies the Born cross section, corresponding to the diagram of Fig. 1(b), is suppressed by the multi-Pomeron exchanges of Fig. 2 by a factor of roughly 0.05. At the LHC the suppression factor⁷ $\langle S^2 \rangle$ is 0.026.

Since the amount of suppression depends on the impact parameter \vec{b} , it leads to a characteristic dependence of the factor S^2 on the angle ϕ between the outgoing protons [18]. This is related to the fact that \vec{b} is the Fourier conjugate to the vector $\vec{q} = \vec{p}_{3\perp} - \vec{p}_{4\perp}$. If the outgoing protons are tagged, then the characteristic peripheral form of the amplitude T^h in \vec{b} -space can be studied experimentally in double-Pomeron-exchange processes by measuring the dependence of the cross section on \vec{q} .

We emphasize that the suppression S^2 , due to absorptive or rescattering corrections, depends not only on the particular process, but also on the kinematical cuts which select events in a given $p_{i\perp}, \phi$ domain. Therefore the suppression S^2 has to be calculated for each particular kinematical configuration.

⁷It is interesting to note that the introduction of the $\vec{p}_{i\perp}$ and angular correlations in (21), (22) raise $\langle S^2 \rangle$ from 0.023 to 0.026.

4.2 Comparison of exclusive diffractive $h(0^\pm)$ Higgs production

So far we have discussed absorptive corrections for $h(0^+)$ production. Here we compare these corrections with those for $h(0^-)$ production. For $h(0^-)$ production we predict a different \vec{q} behaviour. This originates from (15); the Born double-Pomeron-exchange amplitude for process (1) now contains the kinematical factor $(\vec{p}_{3\perp} \times \vec{p}_{4\perp}) \cdot \vec{n}_0$ and this, in turn, implies that the Fourier transform contains the factor $(\vec{b}_1 \times \vec{b}_2) \cdot \vec{n}_0$. Thus the corresponding amplitude $T_{PP}^{h(0^-)}(s_1, s_2, \vec{b}_1, \vec{b}_2)$ tends to zero as \vec{b}_1 or $\vec{b}_2 \rightarrow 0$. As a result, the suppression arising from rescattering is less effective, and the factor S^2 is larger than for $h(0^+)$ production. Also the ϕ distribution is distorted due to absorption.

The effect of the absorptive corrections on the angular correlations ϕ between the outgoing protons was discussed in detail in Ref. [18] for $h(0^+)$ production⁸. There it was shown that the absorptive corrections are largest in the back-to-back configuration where $\vec{p}_{3\perp}$ is directed against $\vec{p}_{4\perp}$, since in this case both $t_1 \simeq -(\vec{k}_\perp + \vec{p}_{3\perp})^2$ and $t_2 \simeq -(\vec{k}_\perp - \vec{p}_{4\perp})^2$ can be minimized simultaneously by the same momentum \vec{k}_\perp transferred in the elastic rescattering, see Fig. 3(b). Thus for $\phi = 180^\circ$ the momentum is transferred mainly through the rescattering amplitude. The suppression factor S^2 was plotted versus ϕ for different choices of $p_{3\perp}$ and $p_{4\perp}$ in Ref. [18]. It was shown that the diffractive dip (which arises from the maximum cancellation between the bare amplitude and rescattering contribution) moves to smaller ϕ as the values of $p_{i\perp}$ are increased.

Here we calculate S^2 as a function of ϕ for $h(0^-)$, as well as $h(0^+)$, exclusive diffractive production. We integrate over the $p_{i\perp}$ of the outgoing protons assuming an $\exp(-b(p_{3\perp}^2 + p_{4\perp}^2))$ behaviour of the Pomeron-proton vertices g_{13} and g_{24} , with $b = 2 \text{ GeV}^{-2}$. We use the two-channel eikonal model of Ref. [16]. For the central vertex we take $(\vec{p}_{3\perp} \times \vec{p}_{4\perp}) \cdot \vec{n}_0$ for $h(0^-)$ production and a constant for $h(0^+)$ production. The results for the suppression factor S^2 are shown in Fig. 5 for $h(0^\pm)$ production of mass 120 GeV at the LHC energy, $\sqrt{s} = 14 \text{ TeV}$. As the azimuthal angle between $\vec{p}_{3\perp}$ and $\vec{p}_{4\perp}$ increases, the first diffractive dip, followed by the second maximum, are evident in the S^2 curves obtained by integrating over all $p_{i\perp}$. The dotted curves show the effect of restricting the outgoing protons to the domain $p_{i\perp} < 0.35 \text{ GeV}$. As expected, the diffractive dip is pushed to larger angles and is barely reached even for the back-to-back configuration, $\phi = 180^\circ$. As we see from Fig. 5 that the survival factor S^2 is about 3–4 times larger for $h(0^-)$ as compared to $h(0^+)$ production. This is a reflection of the more peripheral nature of $h(0^-)$ production. For the same reason the suppression S^2 obtained when integrating over the small $p_{i\perp}$ domain, $p_{i\perp} < 0.35 \text{ GeV}$, is less than when integrating over all $p_{i\perp}$, since it is more weighted to the larger values of the impact parameter b .

Finally in Fig. 6 we show the predictions for the effective luminosity with the absorptive effects included. The original $\sin^2 \phi$ and constant behaviours of $h(0^-)$ and $h(0^+)$, respectively, are distorted first by the $\vec{p}_{3\perp} \cdot \vec{p}_{4\perp}/Q^2$ type corrections from the integration over the gluon loop in Fig. 4, and then by the absorptive effects given by the suppression factors S^2 shown in Fig. 5.

⁸Note that there is a typographical error in eq. (25) of [18], where the last factor should be simply S^2 rather than its second derivative. However the results presented in [18] correspond to the correct definition of F .

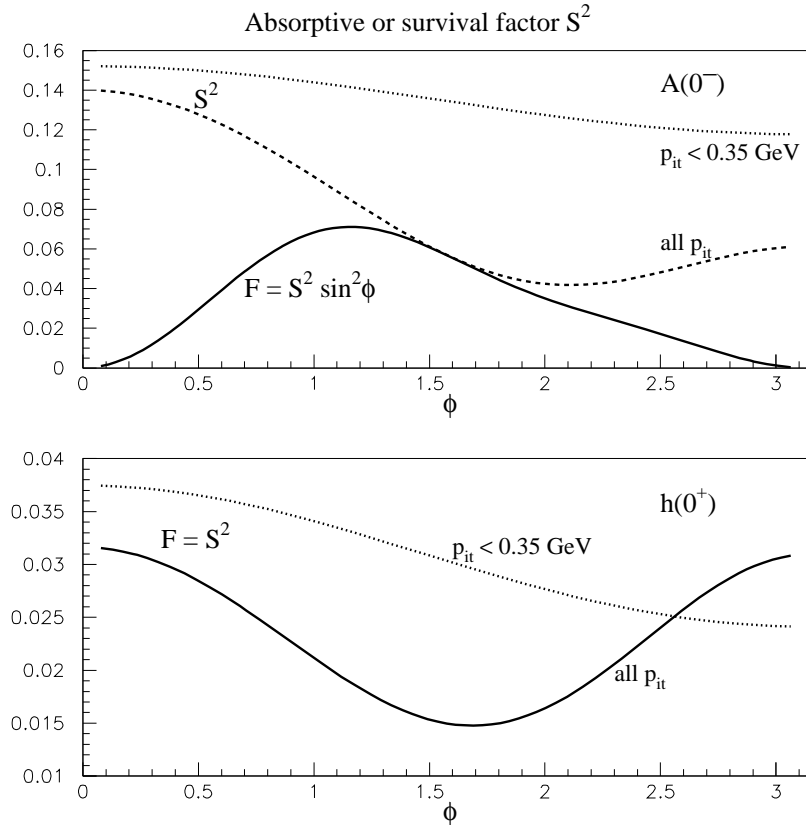


Figure 5: The suppression factors S^2 of $h(0^+)$ and $A(0^-) \equiv h(0^-)$ Higgs production via the process $pp \rightarrow p + h + p$ at the LHC, arising from rescattering effects. The outgoing protons are integrated over (i) all $p_{i\perp}$ and (ii) $p_{i\perp} < 0.35 \text{ GeV}$ (dotted curves). For illustration, the continuous curve for $h(0^-) \equiv A(0^-)$ production includes the general $\sin \phi$ behaviour of the bare amplitude.

5 Consequences for signals in the Higgs sector

We have studied the central *exclusive* diffractive production of bosons via the process $pp \rightarrow p + h + p$, and emphasized that correlations between the outgoing proton momenta reflect the spin-parity of h . As a topical example to illustrate these properties we compared $h(0^+)$ and $A(0^-) \equiv h(0^-)$ Higgs production. In particular, Fig. 6 shows that the dependence on the angle ϕ between the outgoing proton transverse momenta, $\vec{p}_{3\perp}$ and $\vec{p}_{4\perp}$, is different for the natural (0^+) and unnatural (0^-) parity states of h . The comparison with Fig. 4 shows that absorptive effects have significantly distorted the ϕ distributions and, in fact, have increased the difference between the 0^+ and 0^- distributions. Thus this distribution provides a unique possibility to

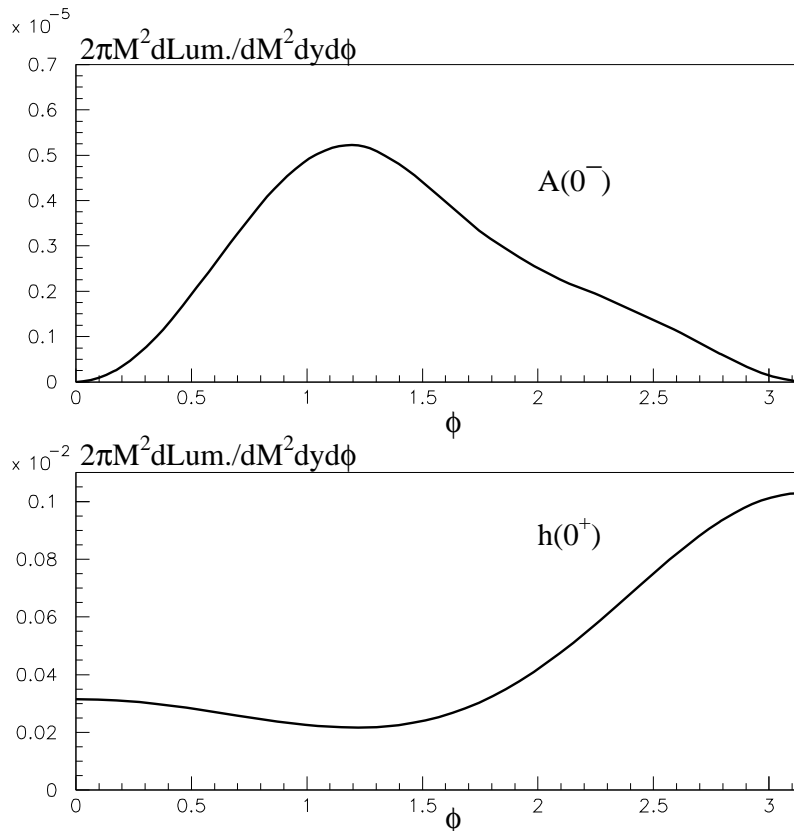


Figure 6: The effective luminosities of the $gg \rightarrow A(0^-) \equiv h(0^-)$ and $h(0^+)$ subprocesses, integrated over the outgoing proton transverse momenta $\vec{p}_{i\perp}$, in the exclusive diffractive processes $pp \rightarrow p + h + p$ at the LHC, with $\sqrt{s} = 14$ TeV, using the MRST99 [30] gluon. Absorptive (or rescattering) effects are included. The curves are for $y = 0$ and Higgs masses of 120 GeV. Comparison with the continuous curves in Fig. 4 shows the suppression of the event rate, and the distortion of the ϕ behaviour due to absorptive effects.

distinguish between 0^+ and 0^- bosons, which, in the case of *inclusive* production⁹, is extremely difficult.

We have seen that the amplitude for the production of unnatural parity ($P = (-1)^{J+1}$)

⁹A proposal, similar in spirit to our approach, can be found in Ref. [33]. The idea is to determine the CP-parity of a Higgs boson by measuring the azimuthal correlations of the tagging (quark) jets which accompany Higgs production via the vector-boson-fusion mechanism. Even if we disregard the possible degradation of the characteristic features of the distribution caused by parton showers and the inclusive environment of the jets, we note that the method is not applicable in some important regions where the couplings of the Higgs to vector bosons are strongly suppressed. Another method to determine the spin-parity of the Higgs, which similarly relies on the vector-boson coupling, was discussed in Ref. [34].

states contains a factor $(\vec{p}_{3\perp} \times \vec{p}_{4\perp}) \cdot \vec{n}_0$. Thus the cross section vanishes as $p_{3\perp}$ or $p_{4\perp} \rightarrow 0$ and vanishes as $\sin^2 \phi$ as $\phi \rightarrow 0$ or π . These properties may be used to suppress the cross section for natural parity ($P = (-1)^J$) production in comparison to that of unnatural parity states. In particular, selecting events with $p_{3\perp}, p_{4\perp} > 0.4$ GeV and $20^\circ < \phi < 120^\circ$ suppresses the 0^+ yield by about a factor of 10, while only decreasing the 0^- cross section by a factor of 2.3. The relative 0^- enhancement may be important as the cross section for the central exclusive production of an $A(0^-)$ boson is quite small, and moreover, in many supersymmetric scenarios, the $h(0^+)$ (and/or $H(0^+)$) and $A(0^-)$ bosons are close in mass.

As a specific example we consider Higgs production in the minimal supersymmetric model (MSSM) with large $\tan \beta$ and $m_A \sim 110\text{--}130$ GeV. In this domain the branching ratios of Higgs-like bosons to vector bosons and photon pairs¹⁰, and the couplings to top quarks, are much suppressed [21], and it becomes problematic to perform a complete coverage of the Higgs boson sector using the conventional inclusive processes. In particular the problem of resolving the signals for different states becomes quite challenging¹¹. On the contrary the cross section, σ_{CEP} , for central exclusive diffractive production in the MSSM is enhanced in comparison with that of the SM. The MSSM (for $\tan \beta = 30$) and SM cross sections, σ_{CEP} , at the LHC energy, are shown in Fig. 7. They have been evaluated using the effective gg luminosities obtained in Section 3 with the absorptive corrections calculated in Section 4.2, see Fig. 6. The normalization factor in (21) is

$$N^2 = \frac{2\pi\Gamma(h \rightarrow gg)}{(N_c^2 - 1)^2 m_H^3} K, \quad (32)$$

where the NLO K factor $\simeq 1.5$ [7] and the number of colours $N_c = 3$. The widths and properties of the Higgs scalar (h, H) and pseudoscalar (A) bosons are calculated using the HDECAY code, version 3.0 [35], with all other parameters taken from Table 2 of [35]; also we take $\text{IMODEL} = 4$, which means the radiative corrections are included according to Ref. [36].

From Fig. 7 we see that the 0^+ Higgs bosons should be accessible at the LHC, via the central exclusive signal, over a wide mass range up to about 250 GeV in this scenario. The enhancement of the MSSM signals is clearly apparent, except near $m_h \simeq 127$ GeV. For example, for the production of a Higgs boson of mass 115 GeV for $\tan \beta = 30$ (or 50) we have

$$\text{Br}(h \rightarrow b\bar{b}) \sigma_{\text{CEP}}^{h(0^+)} \sim 20 \text{ (70) fb}, \quad (33)$$

about 10 (40) times larger than σ_{CEP} in the SM.

For the same parameters, for $A(0^-)$ production we obtain

$$\text{Br}(A \rightarrow b\bar{b}) \sigma_{\text{CEP}}^{A(0^-)} \sim 0.2 \text{ (0.5) fb}. \quad (34)$$

¹⁰The branching ratios of $h, H, A \rightarrow \gamma\gamma$ are less than, or of the order of, $10^{-5}\text{--}10^{-4}$, which is much smaller than in the SM.

¹¹The separation of h and H bosons may be especially difficult for *inclusive* signals, where the mass resolution is usually $\Delta m \gtrsim 10$ GeV, except in the $\gamma\gamma$ and probably $\mu\mu$ modes. However, with forward proton taggers, the *exclusive* signal has the added bonus that a mass resolution of $\Delta m \sim 1$ GeV may be obtained [38].

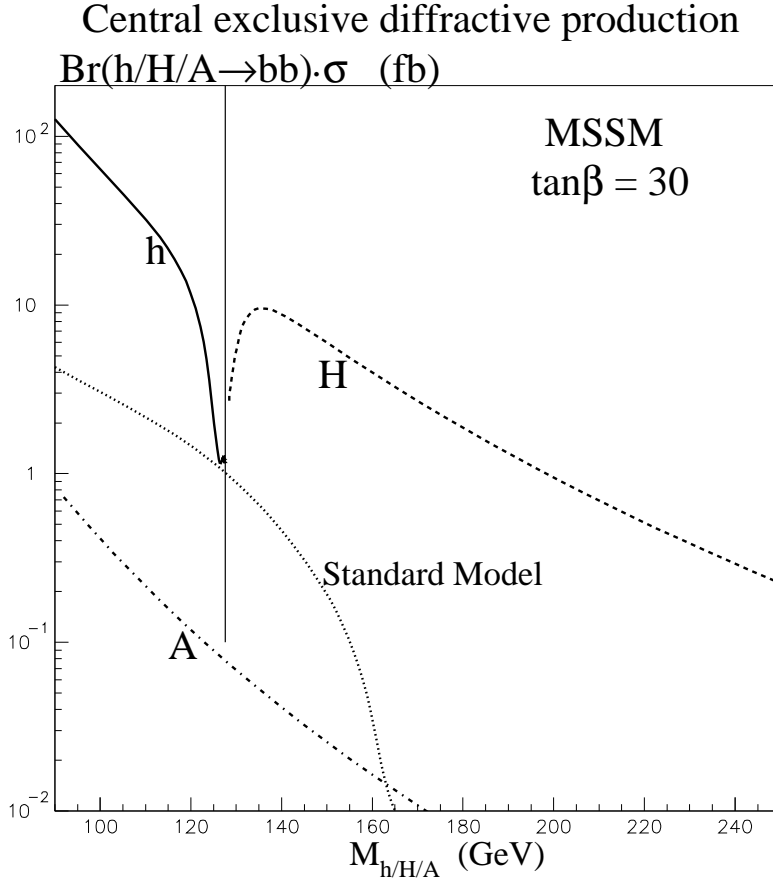


Figure 7: The cross sections times the $b\bar{b}$ branching ratio predicted, for the central exclusive production of $h(0^+)$, $H(0^+)$ and $A(0^-)$ MSSM Higgs bosons (for $\tan\beta = 30$), at the LHC, compared with the SM result. We use the MRST99 [30] gluon distribution. The vertical line separates the mass regime of light $h(0^+)$ and heavy $H(0^+)$ bosons.

However we have emphasized the infrared sensitivity of the *rate* of $A(0^-)$ production. It is possible that a non-perturbative contribution, coming from low values of Q_\perp in (21), may enhance the cross section by a factor of 3 or more. Nevertheless it would be extremely hard to observe the $A(0^-)$ boson under the $h(0^+)$ signal, when the masses are close. A typical mass difference is $m_A - m_h \simeq 2.9$ (1.4) GeV for $\tan\beta = 30$ (50), if $m_A = 115$ GeV. The situation for the observation of the $A(0^-)$ boson is even worse due to the comparatively large expected widths of the Higgs bosons. For instance, if $m_A \sim 90$ –130 GeV and $\tan\beta = 30$, then the widths of the Higgs bosons become of order 2 GeV [20]. On the other hand, proton taggers, with a very accurate missing mass resolution of $\Delta M \simeq 1$ GeV, offer the attractive possibility, not only to separate the h and H bosons, but also to provide a direct measurement of the widths of the h (for $m_h \lesssim 120$ GeV) and the H bosons (if $m_H \gtrsim 130$ GeV). Also we note that by comparing the cross sections of (33) and (34), we see that if a new heavy object were observed in inelastic

events, but not in exclusive central production, it would indicate that it had unnatural parity.

Although the rate of $A(0^-)$ Higgs production is sensitive to contributions from the infrared region, we do not expect a significant change in the qualitative behaviour of the 0^- production amplitude. The reasons are as follows. First, the vanishing of the amplitude as $p_{i\perp} \rightarrow 0$ and/or $\phi \rightarrow 0, \pi$ follows from the general form (15) of the vertex in Regge theory. Second, as a rule the extra ϕ dependence caused by the $\vec{p}_{3\perp} \cdot \vec{p}_{4\perp}$ term is weak, see Fig. 4 for example. Third, in the very extreme case where we use GRV94 partons [37] (which enable us to take a very low infrared cut-off $Q_0^2 = 0.4 \text{ GeV}^2$, but which are known to overestimate significantly the low x gluon), the 0^- Higgs cross section is enhanced, relative to that obtained using MRST99 partons with $Q_0 = 1.3 \text{ GeV}$, by about a factor of 4, but the ϕ and $p_{i\perp}$ dependences are essentially unaltered.

Returning to $h(0^+)$ production, we see, for the example of (33), that already for an LHC luminosity $\mathcal{L} = 30 \text{ fb}^{-1}$, about 600 (2000) bosons are produced. If the experimental cuts and efficiencies quoted in Ref. [38] are imposed, then the signal is depleted by about a factor of 6. This leaves about 100 (400) observable events, with an unaltered background of about 3 events [38] in a $\Delta M = 1 \text{ GeV}$ missing mass bin; which gives an incredible significance for a Higgs signal!

Acknowledgements

We thank Abdelhak Djouadi, Howie Haber, Leif Lonnblad, Risto Orava, Albert de Roeck and Georg Weiglein for valuable discussions. ABK and MGR would like to thank the IPPP at the University of Durham for hospitality. This work was supported by the UK Particle Physics and Astronomy Research Council, by grants INTAS 00-00366, RFBR 01-02-17383 and 01-02-17095, and by the Federal Program of the Russian Ministry of Industry, Science and Technology 40.052.1.1.1112 and SS-1124.2003.2.

References

- [1] K.A. Ter-Martirosyan, Nucl. Phys. **68** (1964) 591.
- [2] WA102 Collaboration: D. Barberis et al., Phys. Lett. **B440** (1998) 225; *ibid.* **B432** (1998) 436; *ibid.* **B427** (1998) 398; *ibid.* **B397** (1997) 339; A. Kirk et al., [arXiv:hep-ph/9810221](https://arxiv.org/abs/hep-ph/9810221).
- [3] A. Bialas and P.V. Landshoff, Phys. Lett. **B256** (1991) 540.
- [4] V.A. Khoze, A.D. Martin and M.G. Ryskin, Phys. Lett. **B401** (1997) 330.
- [5] M.G. Albrow and A. Rostovtsev, [arXiv:hep-ph/0009336](https://arxiv.org/abs/hep-ph/0009336) and references therein.

- [6] V.A. Khoze, A.D. Martin and M.G. Ryskin, Eur. Phys. J. **C14** (2000) 525.
- [7] V.A. Khoze, A.D. Martin and M.G. Ryskin, Eur. Phys. J. **C23** (2002) 311.
- [8] F.E. Close and A. Kirk, Phys. Lett. **B397** (1997) 333.
- [9] J.R. Ellis and D. Kharzeev, arXiv:hep-ph/9811222;
- [10] N.I. Kochelev, arXiv:hep-ph/9902203.
- [11] N.I. Kochelev, T. Morii, B.L. Reznik and A.V. Vinnikov, Eur. Phys. J. **A8** (2000) 405;
N.I. Kochelev, T. Morii and A.V. Vinnikov, Phys. Lett. **457** (1999) 202.
- [12] F.E. Close and G. Schuler, Phys. Lett. **B458** (1999) 127;
F.E. Close, A. Kirk and G. Schuler, Phys. Lett. **B477** (2000) 13.
- [13] E. Shuryak and I. Zahed, arXiv:hep-ph/0302231.
- [14] J.D. Bjorken, Int. J. Mod. Phys. **A7** (1992) 4189, Phys. Rev. **D47** (1993) 101.
- [15] E. Gotsman, E. Levin and U. Maor, Phys. Rev. **D60** (1999) 094011 and references therein.
- [16] V.A. Khoze, A.D. Martin and M.G. Ryskin, Eur. Phys. J. **C18** (2000) 167.
- [17] A.B. Kaidalov, V.A. Khoze, A.D. Martin and M.G. Ryskin, Eur. Phys. J. **C21** (2001) 521.
- [18] V.A. Khoze, A.D. Martin and M.G. Ryskin, Eur. Phys. J. **C24** (2002) 581.
- [19] V.N. Gribov, Sov. Phys. JETP **26** (1968) 414.
- [20] M. Carena and H. Haber, Prog. Part. Nucl. Phys. **50** (2003) 63.
- [21] E. Boos, A. Djouadi, M. Mühlleitner and A. Vologdin, Phys. Rev. **D66** (2002) 055004.
- [22] K.G. Boreskov, Sov. J. Nucl. Phys. **8** (1969) 464 [Yad. Fiz. **8** (1968) 796].
- [23] A.B. Kaidalov and B.M. Karnakov, Sov. J. Nucl. Phys. **3** (1966) 814 [Yad. Fiz. **3** (1966) 1119].
- [24] A.B. Kaidalov and B.M. Karnakov, Sov. J. Nucl. Phys. **11** (1970) 121 [Yad. Fiz. **11** (1970) 216].

- [25] V.A. Khoze, A.D. Martin and M.G. Ryskin, [hep-ph/0006005](#), in *Proc. of 8th Int. Workshop on Deep Inelastic Scattering and QCD (DIS2000)*, Liverpool, eds. J. Gracey and T. Greenshaw (World Scientific, 2001), p.592.
- [26] V.A. Khoze, A.D. Martin and M.G. Ryskin, *Eur. Phys. J.* **C19** (2001) 477, erratum **C20** (2001) 599.
- [27] Feng Yuan, *Phys. Lett.* **B510** (2001) 155.
- [28] A.D. Martin and M.G. Ryskin, *Phys. Rev.* **D64** (2001) 094017.
- [29] A.G. Shuvaev, K.J. Golec-Biernat, A.D. Martin and M.G. Ryskin, *Phys. Rev.* **D60** (1999) 014015.
- [30] A.D. Martin, R.G. Roberts, W.J. Stirling and R.S. Thorne, *Eur. Phys. J.* **C14** (2000) 133.
- [31] CTEQ Collaboration: J. Pumplin et al., *JHEP* **0207** (2002) 012.
- [32] A.D. Martin, R.G. Roberts, W. J. Stirling and R.S. Thorne, *Eur. Phys. J.* **C28** (2003) 455.
- [33] T. Plehn, D. Rainwater and D. Zeppenfeld, *Phys. Rev. Lett.* **88** (2002) 05181.
- [34] S.Y. Choi, D.J. Miller, M.M. Muhlleitner and P.M. Zerwas, *Phys. Lett.* **B553** (2003) 61.
- [35] A. Djouadi, J. Kalinowski and M. Spira, *Comput. Phys. Com.* **108** (1998) 56, [arXiv:hep-ph/9704448](#).
- [36] S. Heinemeyer, W. Hollik and G. Weiglein, [arXiv:hep-ph/0002213](#).
- [37] M. Glück, E. Reya and A. Vogt, *Z. Phys.* **C67** (1995) 433.
- [38] A. De Roeck, V.A. Khoze, A.D. Martin, R. Orava and M.G. Ryskin, *Eur. Phys. J.* **C25** (2002) 391.